


Article

Investigation of Flow and Heat Transfer Performance of Double-Layer Pin-Fin Manifold Microchannel Heat Sinks

Yantao Li ¹, Qianxiang Wang ¹, Minghan Li ¹, Xizhen Ma ², Xiu Xiao ¹ and Yulong Ji ^{1,*} ¹ Marine Engineering College, Dalian Maritime University, Dalian 116026, China² The Boiler & Pressure Vessel Safety Inspection Institute of Henan Province, Zhengzhou 450000, China

* Correspondence: jiyulong@dlnu.edu.cn; Tel.: +86-411-84724306

Abstract: The manifold microchannel (MMC) heat sink is characterized by high heat transfer efficiency, high compactness, and low flow resistance. It can be an effective method for the high-flux removal of high-power electronic components. To further enhance the performance of the MMC, a double-layer pin-fin MMC structure was designed. The thermodynamic properties, including the flow and heat transfer characteristics, were numerically investigated using ANSYS Fluent with deionized water as the working liquid. Compared with the single-layer MMC, the temperature uniformity is better, the pressure drop is lower, and the comprehensive performance is improved at the cost of slightly larger thermal resistance for the double-layer MMC. The geometric effects on the thermodynamic performance were also analyzed. The results show that among the pin-fin structures with round, diamond-shaped, and rectangular cross-sections, the round pin-fins demonstrate the best comprehensive performance and the minimal thermal resistance. Under the same inlet velocity, the thermal resistance is decreased, and the comprehensive performance is first increased and then decreased as the pin-fin size increases. In addition, it is recommended to adopt a larger height ratio for low inlet velocity and a smaller height ratio for high inlet velocity.

Keywords: manifold microchannel; double-layer microchannel; pin-fin; height ratio; temperature uniformity



Citation: Li, Y.; Wang, Q.; Li, M.; Ma, X.; Xiao, X.; Ji, Y. Investigation of Flow and Heat Transfer Performance of Double-Layer Pin-Fin Manifold Microchannel Heat Sinks. *Water* **2022**, *14*, 3140. <https://doi.org/10.3390/w14193140>

Academic Editor: Jinliang Xu

Received: 5 September 2022

Accepted: 27 September 2022

Published: 5 October 2022

Publisher's Note: MDPI stays neutral with regard to jurisdictional claims in published maps and institutional affiliations.



Copyright: © 2022 by the authors. Licensee MDPI, Basel, Switzerland. This article is an open access article distributed under the terms and conditions of the Creative Commons Attribution (CC BY) license (<https://creativecommons.org/licenses/by/4.0/>).

1. Introduction

With the rapid development of micro-electro-mechanical systems, microchannel structures have been widely applied in chemical and biological engineering, microelectronics, aerospace, and especially high-power chip cooling [1–4]. According to Moore's Law, the transistors accommodated on an integrated circuit double about every 18 months [5], and the chip's performance also doubles. Meanwhile, the heat flux of electronic chips also increased sharply. The traditional cooling technology cannot meet the requirements for heat dissipation, which limits the further improvement of the chip's performance [6]. Harpole and Eninger et al. [7] proposed the manifold microchannel (MMC), which has excellent thermal performance. It is expected to become an effective high-power chip cooling method.

Traditional microchannel heat sinks have several disadvantages, including poor temperature uniformity and high pressure drop. Therefore, the study of novel structures and patterns of flow channels has been conducted to enhance the thermal performance of traditional microchannel heat sinks. Li et al. [8] conducted an experimental survey of zigzag microchannels. They found that the zigzag channel has the minimum pressure drop and the best thermal performance at an attack angle of 30°. Zhai et al. [9] proposed a fan-shaped microchannel and concluded that its thermal performance is better than that of rectangular microchannels. Xu et al. [10] performed a simulation study on a tree-shaped microchannel heat sink. It was found that the tree-shaped structure has better temperature uniformity, and the cooling effect of the seven-level tree-shaped microchannel has the best minimal

pressure drop. Li et al. [11] conducted an experimental research study on a bidirectional counter-flow microchannel heat sink. The results display that its heat transfer capacity was better and the pressure drop was reduced compared to the rectangular microchannel.

Some other researchers proposed a pin–fin structure to replace the traditional straight microchannel. The heat transfer capacity can be improved due to the larger heat transfer area and enhanced flow turbulence. Current research studies have focused on the arrangement and geometric parameters of pin–fin as they are critical parameters affecting the flow and thermal performance. Alam et al. [12] proposed a triangular micro-pin–fin structure, which significantly improved the heat sink's heat dissipation capacity. Yang et al. [13] compared the heat transfer characteristics of heat sinks with five micro-pin–fin structures through a combined simulation and experimental study. It showed that the cylindrical micro-pin–fin structure demonstrates a minimum pressure drop. Xia et al. [14] proposed a rhomboid-shaped micro-pin–fin design. The experimental results show that the thermal performance of this structure is better compared with the cylindrical structure at high Re . Ambreen et al. [15] investigated the effect of pin–fin shapes on heat transfer performance and concluded that the round pin–fins have the best thermal performance.

Double-layer microchannels proposed by Vafai et al. [16] have attracted the interest of many researchers. Many studies have been engaged in improved structures for heat transfer enhancement. The thermal performance of single-layer and double-layer heat sinks was compared by Hu et al. [17], and the authors claimed that the double-layer structure shows better temperature uniformity. Lin et al. [18] investigated the thermal transfer capacity of a double-layer microchannel structure under a heat flux of 100 W/cm^2 and a pump power of 0.2 W . Compared with a single-layer structure, the thermal resistance decreased by about 11% and the temperature difference was lowered from 4.6 K to 0.5 K . Shen et al. [19] proposed a novel X-structured double-layer microchannel heat sink. It was found that this structure displays better temperature uniformity compared with the traditional double-layer microchannel heat sinks. Chen et al. [20] conducted a simulation study on a double-layer trapezoidal microchannel heat sink with a pyramidal perturbation structure. They found that the novel design demonstrates the best thermal performance when the bottom-to-height ratio of the perturbation structure is 0.6 and the spacing is $300 \mu\text{m}$. Zhang et al. [21] proposed a double-layer microchannel with fins of different thicknesses in the upper and lower layers. The results found that the heat transfer performance is improved and the pressure drop is reduced for thicker fins in the lower layer.

Recently, the MMC heat sink has become a research hotspot due to its excellent thermal performance. The MMC structure comprises a manifold divider layer and a microchannel layer, as illustrated in Figure 1. The upper manifold divider layer provides numerous inlet and outlet channels, which are alternately distributed in the length direction of the bottom microchannel. After flowing through the inlet of the manifold structure, the liquid ejects downwards to the bottom surface. Then, the liquid turns direction and flows in the parallel microchannels to dissipate the heat. Finally, the liquid flows upward at the outlet of the manifold divider layer. The manifold structure of the MMC divides the entire long microchannels into many short microchannel units, which reduces the effective length of the flow channel, thereby reducing the pressure drop of the overall structure. Meanwhile, the thermal boundary layer is difficult to fully develop due to a reduction in the effective flow length and the multi-inlet jet effect, leading to a better heat thermal performance. Most of the studies on the MMC focus on structural assembly and optimization. Pan et al. [22] numerically studied the geometric structure effect on the MMC performance. It was found that there is an optimal aspect ratio, which demonstrates the most efficient heat transfer performance. Gan et al. [23] performed a simulation investigation on a novel orifice MMC sink. They found that the temperature uniformity of the novel orifice MMC structure has been dramatically improved. Yang et al. [24] proposed a MMC structure with secondary oblique channels. The optimal structure was obtained through a genetic algorithm, and the numerical simulation results show that this structure has better thermal performance than the traditional MMC. Gilmore et al. [25] proposed an open MMC structure. A smaller

pressure drop was obtained at the cost of lower heat transfer performance compared to the traditional MMC. Erp et al. [26] directly etched the MMC structure on the silicon-based chips, which decreased the thermal resistance since the contact layer between the heat source and the heat sink was removed. This result showed that the MMC structure has excellent application prospects in chip cooling.

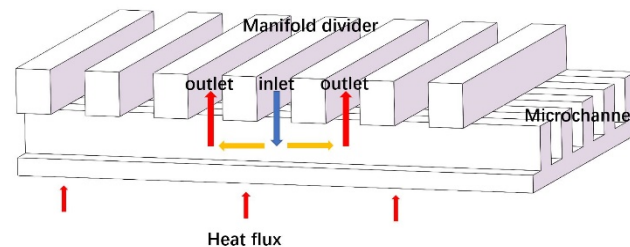


Figure 1. A schematic diagram of an ordinary MMC.

As discussed above, although the pin–fin structure can enhance heat transfer, it also increases the pressure drop. The double-layer heat sinks can reduce the pressure loss at the cost of higher thermal resistance. The MMC heat sink can improve temperature uniformity with a lower pump power. In the current studies, the heat transfer improvement of the MMC is generally achieved at a higher pressure drop penalty. To solve this problem, this work designs a double-layer pin–fin MMC structure by combining the advantages of double-layer and pin–fin structures to enhance heat transfer and improve the temperature uniformity at a lower pressure drop. On this basis, the flow and thermal characteristics of the double-layer pin–fin MMC structure are numerically investigated and the influences of the pin–fin shape, pin–fin size, and height ratio of the upper and lower microchannel layer are discussed.

2. Methodology

2.1. Geometric Model of the Double-Layer Pin–Fin MMC

Figure 2 illustrates the geometric scheme of the double-layer pin–fin MMC. The difference from the traditional MMC structure is that it has two microchannel layers, and the discontinuous microchannels in the microchannel layers are formed with a pin–fin structure. As shown in Figure 2, the cold liquid is injected downwards onto the upper and lower microchannel layers after flowing through the manifold inlet. Then, the liquid spreads along the microchannels among the regularly arranged pin–fins for heat exchange. The liquid flow direction in the microchannel layer is shown in Figure 3. Finally, the hot liquid flows upwards and exits from the outlet layer.

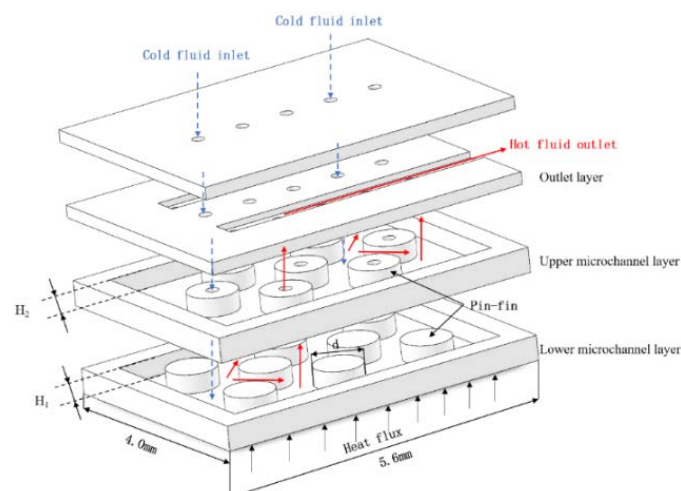


Figure 2. The structure of the double-layer pin–fin MMC.

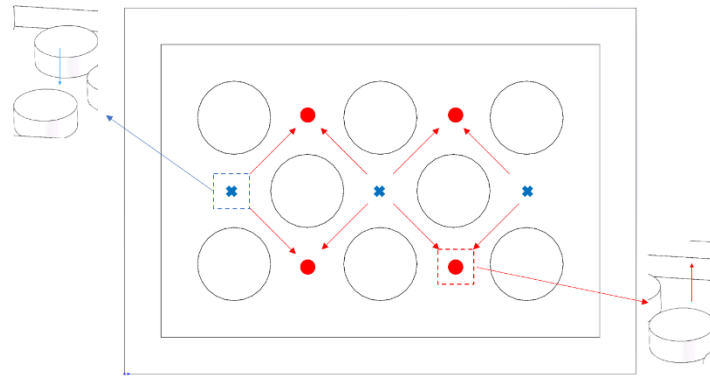


Figure 3. A schematic diagram of the liquid flow direction in the lower microchannel layer.

2.2. Governing Equations and Boundary Conditions

The governing equations for the liquid region are shown below.

Continuity equation:

$$\frac{\partial}{\partial x_i}(\rho u_i) = 0 \quad (1)$$

Momentum equation:

$$\frac{\partial}{\partial x_i}(\rho u_i u_j) = \frac{\partial}{\partial x_i} \left[\mu \left(\frac{\partial u_j}{\partial x_i} + \frac{\partial u_i}{\partial x_j} \right) \right] - \frac{\partial p}{\partial x_j} \quad (2)$$

Energy equation:

$$\frac{\partial}{\partial x_i}(\rho c_p u_i T) = \frac{\partial}{\partial x_i} \left(\lambda \frac{\partial T}{\partial x_i} \right) \quad (3)$$

where c_p , μ , ρ , and λ are the specific heat capacity at a constant pressure, the viscosity, the density, and the thermal conductivity of the liquid, respectively. i and j are the tensor index symbols, which are equal to 1, 2, and 3 in Cartesian coordinates.

To conduct numerical simulation, the commercial software Ansys Fluent 2020R2 is adopted, and deionized water is used as the working liquid. The inlet temperature and pressure are set at 293.15 K and 0.1 MPa, respectively. The inlet velocity covers 1.2 m/s to 3.6 m/s. Due to the turbulence caused by numerous pin-fins and the multi-inlet jet effect, there is a possibility of local turbulent flow despite the corresponding Re values calculated for microchannels being lower than the transitional range of 2500 [27]. The reliable k - ϵ turbulence model is adopted, and the boundary conditions are set as a velocity inlet and a pressure outlet. A uniform heat source of 100 W/cm² is maintained at the bottom boundary. All simulation works are assumed to be performed under steady-state conditions, and the liquid flow is incompressible.

2.3. Data Reduction

The effective thermal resistance of the MMC is calculated as:

$$R_{eff} = \frac{T_s - T_{in}}{Aq} \quad (4)$$

where T_s is the average bottom surface temperature of the MMC, T_{in} is the inlet temperature, A is the effective heating area, and q is the heat flux.

The temperature uniformity is assessed by calculating the temperature difference between the maximum and the minimum temperature at the bottom surface of the MMC:

$$\Delta T = T_{max} - T_{min} \quad (5)$$

where T_{max} and T_{min} are the maximum and the minimum temperatures, respectively.

The comprehensive performance index of the MMC can be described by the factor ζ [28]:

$$\zeta = \frac{j}{f} \quad (6)$$

where j and f are the Colburn factor and the Fanning friction factor, which can be obtained using the following formula:

$$j = \frac{Nu}{RePr^{\frac{1}{3}}} \quad (7)$$

$$f = \frac{\Delta PD}{2u^2\rho L} \quad (8)$$

where u , ρ , L , and ΔP are the inlet velocity, the deionized water density, the overall length of the flow channel, and the pressure drop, respectively. The hydraulic diameter of the flow channel D is obtained by the following equation.

$$D = \frac{4A}{p} = \frac{4A \times L}{p \times L} = \frac{4V}{S} \quad (9)$$

where V , p , and S are the volume of the liquid domain, the wetted perimeter, and the wetted area of the flow channel, respectively.

The Reynolds number and the Prandtl number can be calculated as follows:

$$Re = \frac{\rho u D}{\mu} \quad (10)$$

$$Pr = \frac{\mu C_p}{\lambda} \quad (11)$$

where μ , C_p , and λ are the dynamic viscosity coefficient, the specific heat capacity at constant pressure, and the thermal conductivity of the deionized water, respectively.

The Nusselt number is:

$$Nu = \frac{hD}{\lambda} \quad (12)$$

where h is the convective heat transfer coefficient:

$$h = \frac{q}{(T_s - T_{av})} \quad (13)$$

where T_{av} is the average temperature

$$T_{av} = \frac{T_{in} + T_{out}}{2} \quad (14)$$

where T_{in} and T_{out} are the inlet and outlet liquid temperatures, respectively.

2.4. Grid Independence Verification and Simulation Method Validation

FLUENT meshing is used to generate polyhedral meshes to ensure the accuracy of numerical calculations. The advantage of the polyhedral mesh is that it can capture delicate geometric features, although the number of meshes is significantly reduced compared to the tetrahedral mesh. A higher mesh generation rate compared with ICEM makes FLUENT meshing more suitable for liquid simulation and preprocessing complex geometric shapes. As shown in Figure 4, the fluid domain meshes near the walls are set to five refined boundary layers. Figure 5 shows the grid independence verification results. It can be seen that the Nu and pressure drop barely change as the grid number exceeds 594,758. To save computing resources, the following simulations are performed with the number of grids set at 594,758.

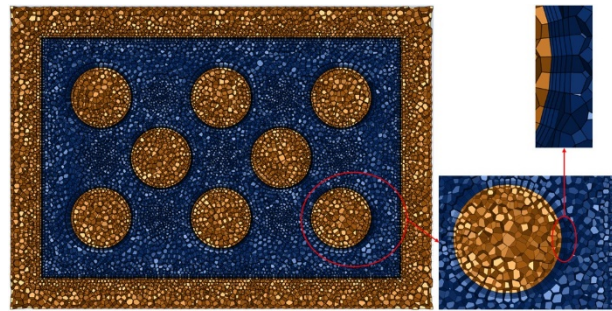


Figure 4. Polyhedral grid generation in the lower microchannel layer.

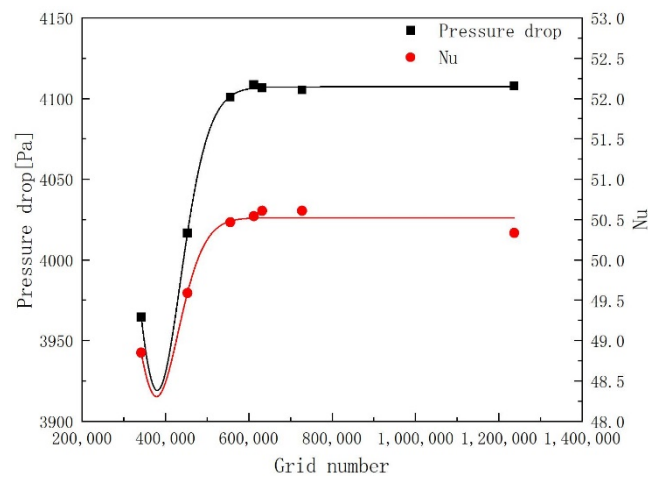


Figure 5. Grid independence analysis.

The numerical simulation method is validated by comparing the calculation results with the experimental data from Drummond [29]. The geometric parameters of the single-layer MMC and the experimental conditions in Drummond’s experiment are displayed in Table 1 and Figure 6, respectively. In the verification experiment, the heat sink material is silicon and the working liquid is HFE7100. The set convergence condition is that the residual error is less than 10^{-12} and the convergence time is 1000 steps. The calculation results are compared with the experimental data in Figure 7. Apparently, the calculated average temperature of the heat sink shows the same trend as the experimental data in a single-phase heat transfer, and the maximum deviation is lower than 1%. Therefore, the reliability of the simulation method in this study is validated.

Table 1. Summary of the validation model parameters.

Parameter	Variable	Values
microchannel width	w_c	16 μm
microchannel rib width	w_r	16 μm
microchannel depth	l_d	150 μm
chip base thickness	l_b	150 μm
inlet width	w_{in}	500 μm
outlet width	w_{out}	250 μm
divider width	w_{div}	250 μm
mass flow rate	G	1300 $\text{kg}/(\text{m}^2 \cdot \text{s})$
heat flux	q	0–75 W/cm^2
inlet temperature	T_{in}	332 K

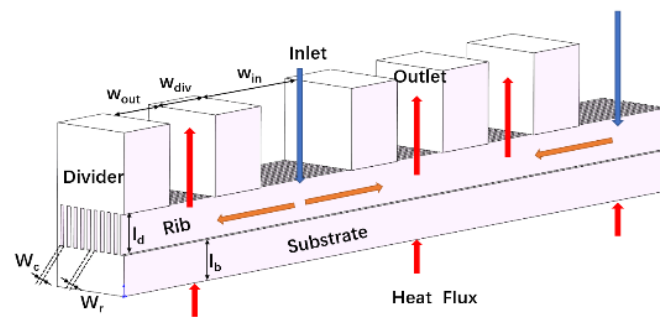


Figure 6. A schematic diagram of single-layer structure from Drummond [29].

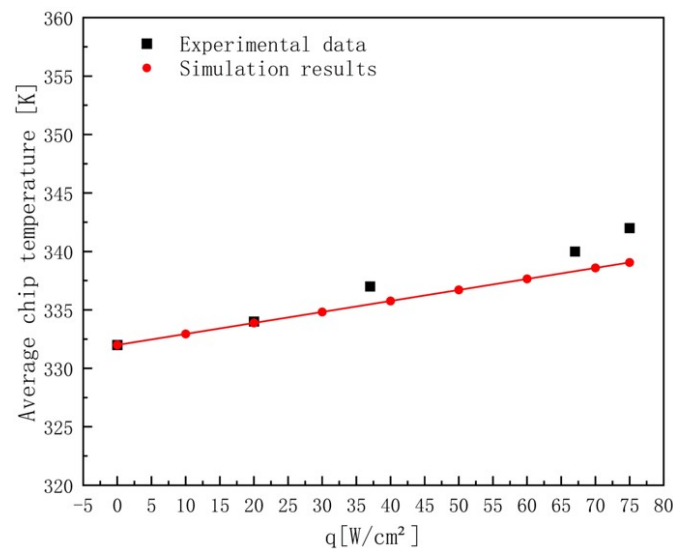


Figure 7. Simulation method validation.

3. Simulation Results and Discussion

3.1. Comparison of the Flow and Heat Transfer Performance of the Double-Layer and Single-Layer Pin-Fin MMC

The flow and thermal performances of the double-layer and single-layer pin-fin MMC are obtained and compared in this section. For both, the height of the microchannel layer is 0.3 mm, and the pin-fin has a round cross-section and a diameter of 0.8 mm. The difference is that the double-layer MMC owns two microchannel layers while the single-layer structure lacks the upper microchannel layer, as depicted in Figure 2. The other detailed working conditions, such as the inlet velocity and temperature, are referred to in Section 2.2.

Figure 8 exhibits the thermal resistance, the maximum temperature difference, the pressure drops, and the comprehensive performance of both the double-layer and single-layer pin-fin MMC. As depicted in Figure 8a, the thermal resistance of the double-layer MMC is 2.1% to 5.7% higher compared with the single-layer heat sink. Since the flow area in the microchannel layer of the double-layer MMC is doubled compared with the single-layer heat sink, the latter has a much higher flow velocity in the microchannel layer under the same total inlet velocity. A higher flow velocity in the single-layer MMC contributes to the multi-inlet jet effect and flow turbulence, which destroy the thermal boundary and enhance the convective heat transfer. Therefore, the single-layer heat sink demonstrates a slightly lower thermal resistance. Figure 8b indicates that the maximum temperature difference of the double-layer heat sink is lower compared with the single-layer structure. This is because the lower microchannel layer can be further cooled by the working liquid in the upper layer for the double-layer MMC, thus achieving better temperature uniformity. In the meantime, the maximum temperature differences for both structures decrease with an increase in the inlet velocity. This is because the higher velocity can improve the convection

heat transfer in the flow dead zone and decrease the temperature difference of the MMC. Figure 8c shows that the pressure loss of the double-layer heat sink is lower compared with the single-layer structure. Specifically, the pressure drop can be reduced by up to 35.2%. This is because under the same total inlet velocity, the doubled flow area in the double-layer MMC causes lower velocities in each microchannel layer, resulting in a lower pressure drop. Figure 8d shows that the double-layer MMC demonstrates better comprehensive performance compared with the single-layer MMC. This result is synonymous with the fact that the double-layer MMC can sharply reduce the pressure loss at the cost of slightly higher thermal resistance.

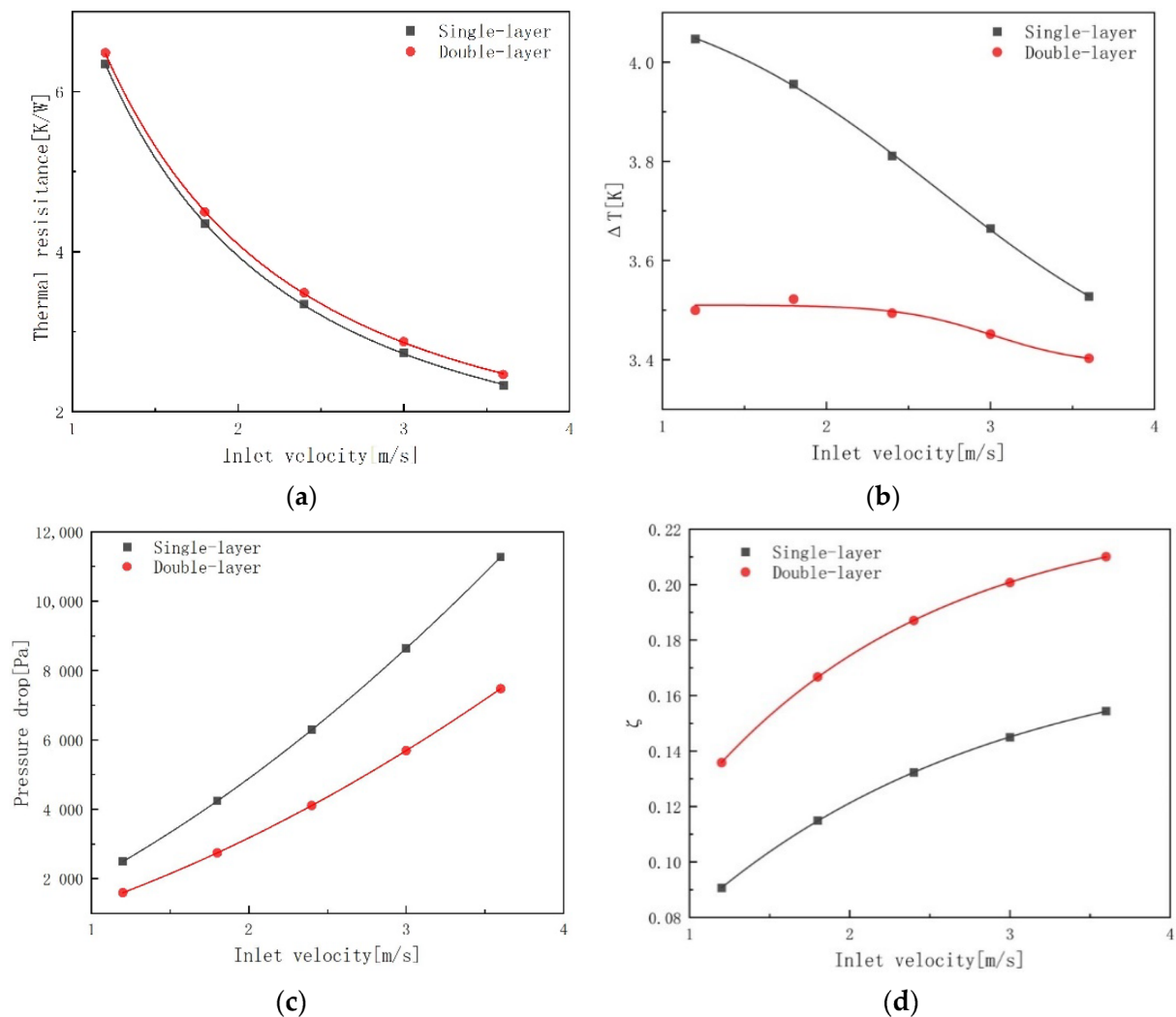


Figure 8. Comparison of flow and heat transfer performance of the double-layer and single-layer pin-fin MMC: (a) thermal resistance; (b) maximum temperature difference; (c) pressure drops; and (d) comprehensive performance.

3.2. Geometric Effects on the Flow and Heat Transfer Performance of the Double-Layer Pin-Fin MMC

3.2.1. Pin-Fin Shape

The flow and thermal characteristics of the double-layer MMC with various pin-fin shapes are analyzed in this section. Figure 9 illustrates the pin-fins with round, diamond-shaped, and rectangular cross-sections. For comparing different pin-fin shapes, the circumscribed circle diameters of the diamond and rectangle are set to be the same as that of the round shape.

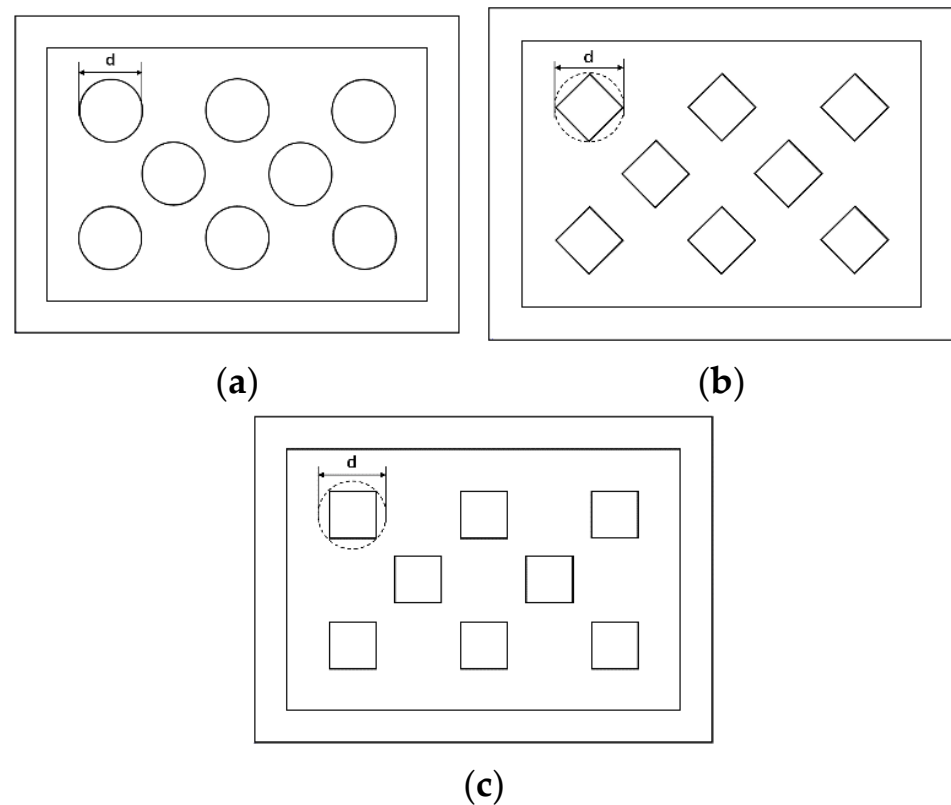


Figure 9. Cross-section of pin-fins: (a) round; (b) diamond; and (c) rectangle.

Figure 10 shows the thermal resistance, maximum temperature difference, pressure drops, and comprehensive performance of the double-layer MMC with three pin-fin shapes mentioned above. As shown in Figure 10a, the thermal resistance for pin-fins with round, diamond-shaped, and rectangular cross-sections decreases with an increase in the inlet velocity. The convective heat transfer is enhanced as the inlet velocity increases, leading to a decreased average temperature. Therefore, the thermal resistance of the MMC also decreases. Moreover, the thermal resistance of the MMC with the round-shaped pin-fin is lower compared to the other pin-fin shapes. This is because the effective flow channel area among the round pin-fins is smaller, and the flow velocity is faster, leading to a higher convective heat transfer coefficient and a lower thermal resistance for the round pin-fin under the same inlet velocity. Figure 10b shows that the maximum temperature difference for the diamond-shaped pin-fin is higher compared with the others. The velocity contour shown in Figure 11 proves that the local velocity around the diamond-shaped pin-fin is lower, resulting in a poor local heat transfer. Thus, the temperature uniformity for the diamond-shaped pin-fin deteriorates. Figure 10c shows that the pressure drops increase with an increase in the flow velocity for three pin-fin shapes. This is because increasing the flow velocity enhances the jet effect and flow turbulence, causing a higher frictional resistance. However, the pressure drops for different pin-fin shapes hardly change under the inlet velocity. This is because the average flow velocity for three pin-fin shapes is similar. The pin-fin shape almost has no effect on the pressure drops. Figure 10d indicates that the comprehensive performance for all pin-fin shapes increases as the inlet velocity increases. The pin-fin with a round cross-section demonstrates the best comprehensive performance. This is because the convective heat transfer for round pin-fins is enhanced due to a higher local velocity in smaller flow passages formed by the round pin-fins. Meanwhile, the pressure drops caused by different pin-fin shapes are similar, which means that the comprehensive performance of the pin-fin with a round cross-section is the best.

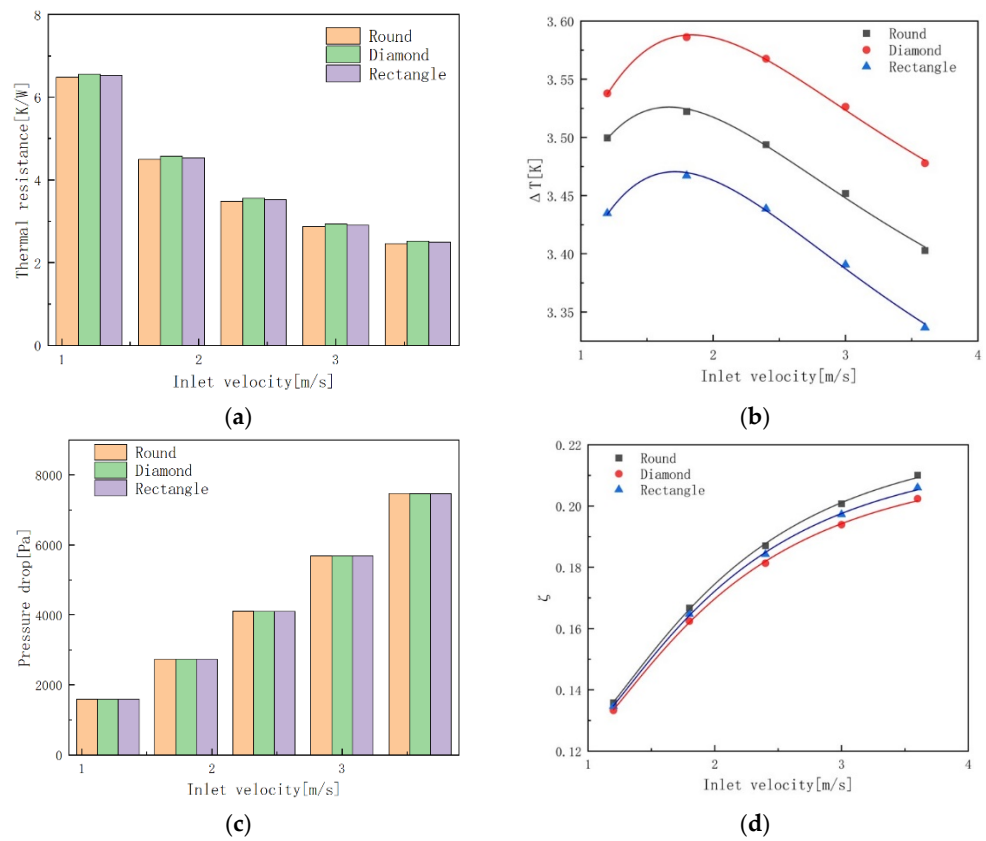


Figure 10. Flow and heat transfer characteristics of the double-layer MMC with different pin-fin shapes: (a) thermal resistance; (b) maximum temperature difference; (c) pressure drops; and (d) comprehensive performance.

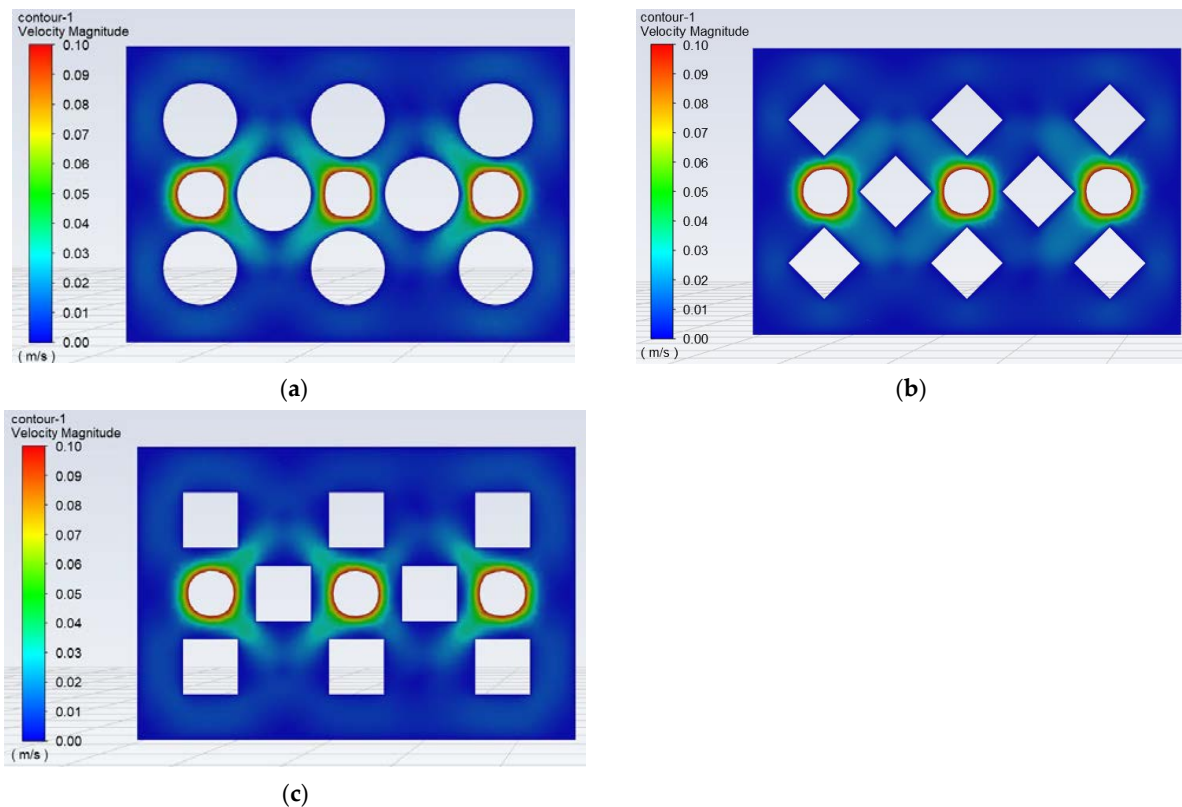


Figure 11. Velocity contour in the lower microchannel layer: (a) round; (b) diamond; and (c) rectangle.

3.2.2. Pin-Fin Size

This section analyzes the flow and thermal characteristics of the double-layer MMC with various pin-fin sizes. Since the pin-fin with a round cross-section demonstrates the best comprehensive performance, it is employed in this section. The diameter of the round cross-section ranges from 0.4 to 1.1 mm, while the other geometric parameters stay constant.

Figure 12 displays the thermal resistance, the maximum temperature difference, the pressure drops, and the comprehensive performance of the double-layer MMC with various pin-fin sizes. Figure 12a shows that despite different pin-fin sizes, the thermal resistance of the MMC decreases as the inlet velocity rises. Meanwhile, the larger the pin-fin size, the lower the thermal resistance. As the pin-fin size increases, the space among the pin-fins becomes smaller, which enlarges the flow velocity and enhances the convective heat transfer. Therefore, the thermal resistance of the MMC reduces as the inlet velocity and the pin-fin size both increase. Figure 12b shows that the maximum temperature difference for all pin-fin sizes slightly decreases with an increase in the inlet velocity. This outcome agrees with a previous study. The maximum temperature difference also decreases with an increase in the pin-fin size. This is because a larger pin-fin size leads to smaller flow passages and a higher flow velocity in the microchannel layer, which enhances the local heat transfer for the flow dead zone and improves the temperature uniformity of the MMC heat sinks. Figure 12c shows that for the pin-fin diameter ranging from 0.4 to 1.0 mm, the pressure drops of the heat sink hardly change. However, once the pin-fin size exceeds 1 mm, the pressure drops increase sharply. This is because when the pin-fin size exceeds 1 mm, the flow area among the pin-fins is too small, resulting in a sudden increase in pressure drops. Figure 12d shows that the comprehensive performance of the double-layer MMC with different pin-fin sizes is significantly enhanced with an increase in the inlet velocity. Meanwhile, the comprehensive performance increases with an increase in the pin-fin size. This suggests that the heat transfer enhancement could overcome the pressure drop penalty caused by increasing pin-fin sizes. However, when the pin-fin size reaches 1.1 mm, the comprehensive performance of the pin-fin MMC significantly decreases due to a sharply increased pressure drop. This indicates that properly increasing the pin-fin size could enhance the comprehensive performance of the pin-fin MMC. However, there is a critical diameter at which comprehensive performance begins to decrease.

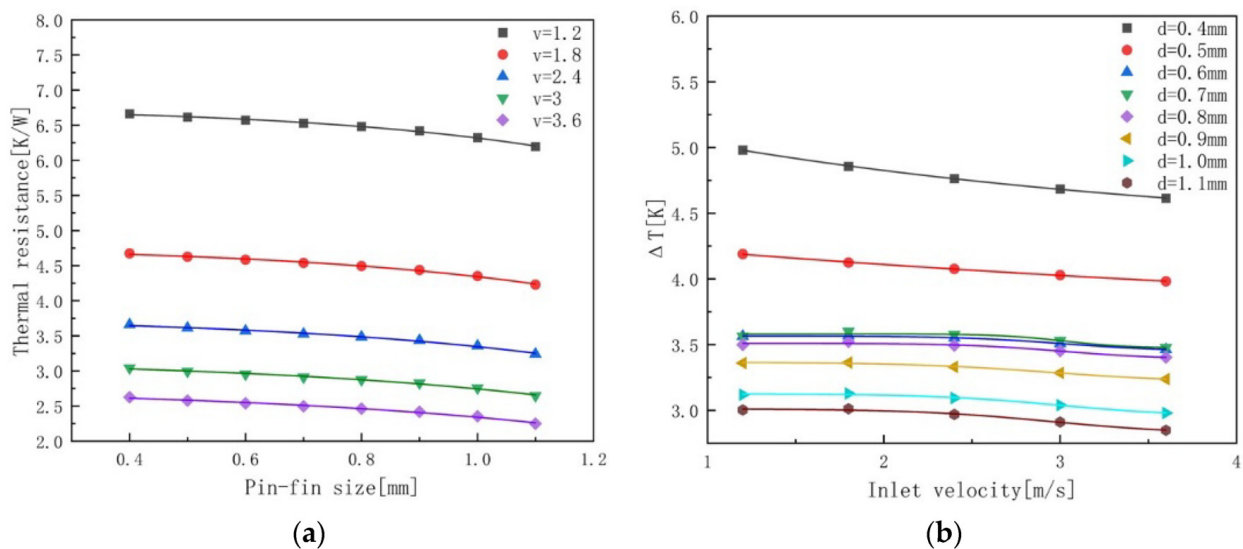


Figure 12. Cont.

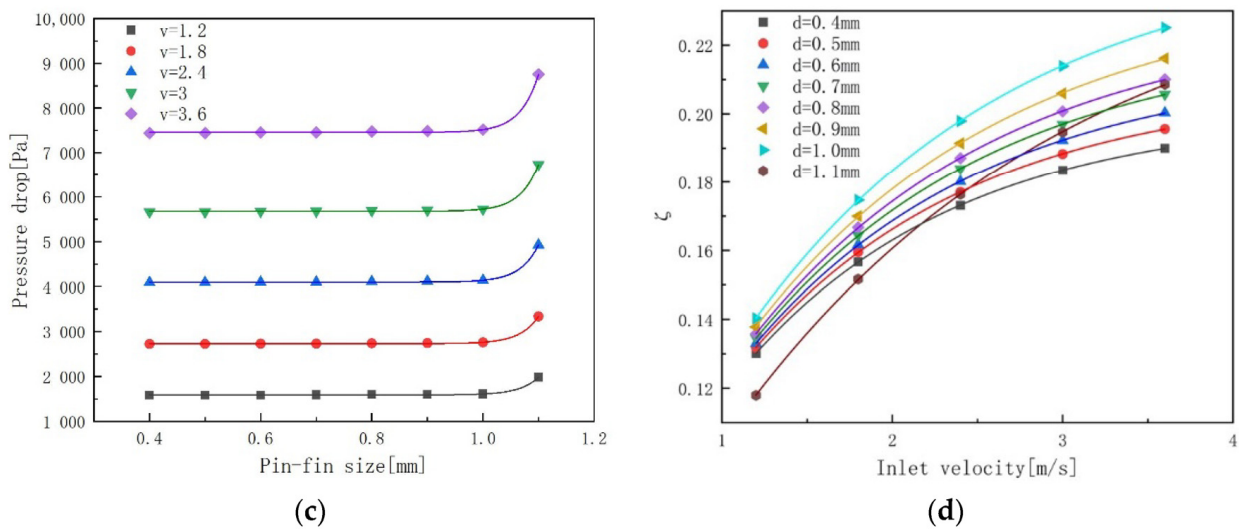


Figure 12. Flow and heat transfer performance of the double-layer MMC with various pin-fin sizes: (a) thermal resistance; (b) maximum temperature difference; (c) pressure drops; and (d) comprehensive performance.

3.2.3. Height Ratio

The effects of the height ratio are discussed in this section. Here, the height ratio, α , refers to the ratio of the upper layer height to the lower layer height ($\alpha = H_2/H_1$, as illustrated in Figure 2), which is adjusted by changing the upper layer height and keeping the lower layer height constant. α changes from 0.4 to 1.2.

Figure 13 shows the flow and thermal characteristics for the double-layer MMC with different height ratios. Figure 13a,b show that the thermal resistance and the maximum temperature difference for all height ratios decrease with an increase in the inlet velocity, which agrees with the previous study. However, the maximum temperature difference and thermal resistance increase with an increase in the height ratio. Since the liquid flow in the upper and lower microchannel layers works in parallel in this work, the mass flow rate in the upper microchannel layer increases, and that in the lower microchannel layer decreases with an increase in the upper layer height. Theoretically, more heat is removed by the liquid in the lower layer as it directly contacts the heat source [30]. A reduced flow rate in the lower layer results in a higher thermal resistance and maximum temperature difference. Figure 13c shows that the pressure drops decrease with an increase in height ratios under the same inlet velocity. This is a product of the fact when the flow area increases as the upper layer height increases, it reduces the average flow velocity and the pressure drops. Figure 13d shows that the comprehensive performance for all height ratios increases with an increase in the inlet velocity. However, the comprehensive performance increases with an increase in the height ratios at lower velocities, while the situation is opposite at higher velocities. With the decreased height ratio, the liquid velocity in each microchannel layer increases, causing a higher pressure drop but a larger heat transfer coefficient. It is observed that under a higher inlet velocity, the heat transfer enhancement could overcome the cost of pressure drop caused by a decreased height ratio. Therefore, the comprehensive performance improves with a decreased height ratio at a higher inlet velocity. On the contrary, the comprehensive performance decreases with a decrease in the height ratio at a lower inlet velocity. Thus, a larger height ratio for a low inlet velocity and a smaller height ratio for a high inlet velocity are recommended.

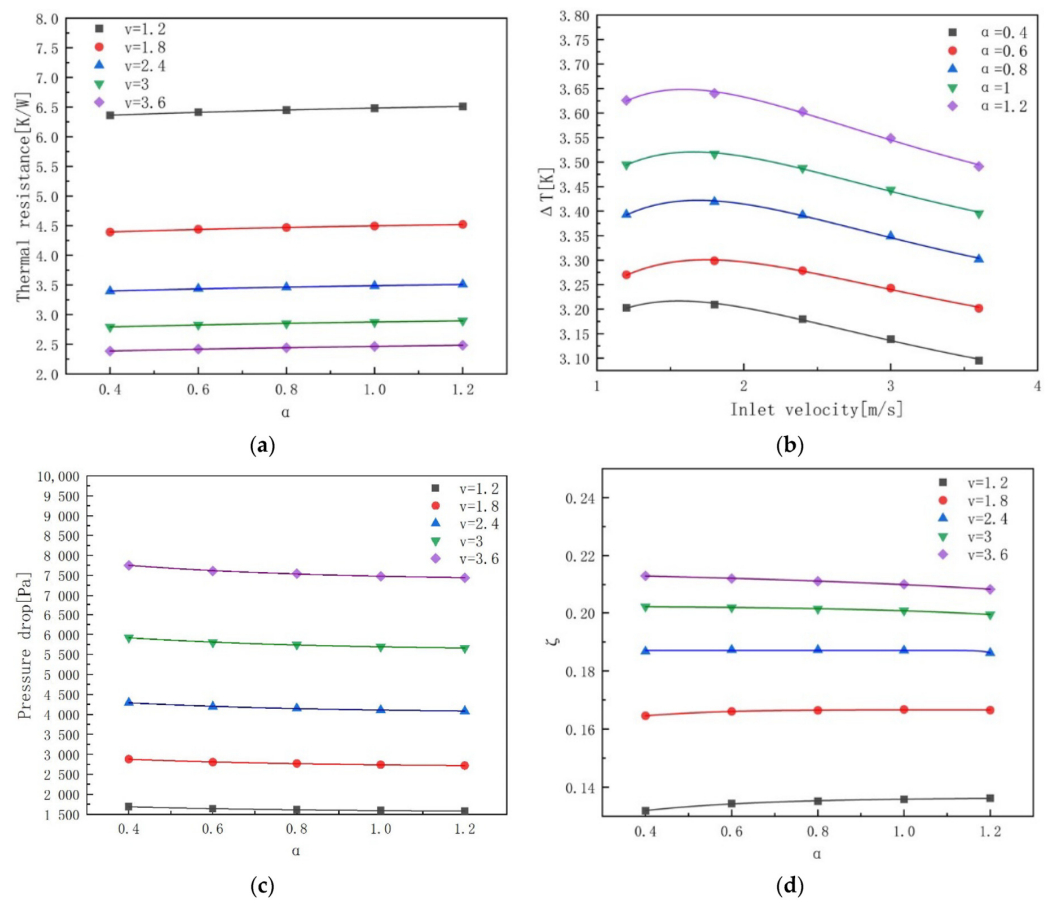


Figure 13. Flow and heat transfer performance of the double-layer MMC with various height ratios: (a) thermal resistance; (b) maximum temperature difference; (c) pressure drops; and (d) comprehensive performance.

4. Conclusions

In this study, a double-layer pin–fin MMC structure is designed, and its flow and thermal performance are studied using ANSYS Fluent. By taking deionized water as the working liquid, the present work comes to the following conclusions.

(1) Compared with the single-layer MMC, the double-layer heat sink demonstrates lower pressure drop, better temperature uniformity, and improved comprehensive performance at the cost of slightly larger thermal resistance.

(2) Among the pin–fin structures with round, diamond-shaped, and rectangular cross-sections, the round pin–fin structure demonstrates minimal thermal resistance and the best comprehensive performance, although its temperature uniformity is relatively poor.

(3) Under the same inlet velocity, the thermal resistance is decreased, and the comprehensive performance is first increased and then decreased as the pin–fin size increases.

(4) To achieve better flow and heat transfer performance, the employment of a larger height ratio at a low inlet velocity and a smaller height ratio at a high inlet velocity is recommended.

(5) Further study on the effect of manifold arrangements on the double-layer MMC is advised. Moreover, the performance of the proposed two-layer MMC should be experimentally validated in the future.

Author Contributions: Conceptualization, Y.L. and Q.W.; methodology, M.L. and X.M.; validation, Y.L.; resources, Y.L.; writing—original draft preparation, Q.W.; writing—review and editing, Y.L., X.X. and Q.W.; supervision, Y.L. and Y.J.; project administration, Y.J.; funding acquisition, Y.L., Y.J. and X.M. All authors have read and agreed to the published version of the manuscript.

Funding: This research was funded by the National Key Research and Development Program of China (2019YFE0116400), the National Natural Science Foundation of China (52006023), the Liaoning Revitalization Talents Program of China (XLYC1807117), the Dalian Outstanding Scientific and Technological Talents Program of China (2020RJ03), the Fundamental Research Funds for the Central Universities (3132022649), and the Science and Technology Plan Project of Administration for Market Regulation of Henan Province (2020sj62).

Data Availability Statement: Not applicable.

Acknowledgments: The authors appreciate Wei Zhang, Chunrong Yu, Zhang Liu, Tai Liu, and Yunxiao Yang for their support and cooperation.

Conflicts of Interest: The authors declare no conflict of interest.

Nomenclature

A	heating area (m^2)
C_p	specific heat capacity at constant pressure ($\text{J}/\text{kg}\cdot\text{K}$)
d	diameter of pin-fin (m)
D	hydraulic diameter (m)
f	Fanning friction factor (-)
h	heat transfer coefficient ($\text{W}/\text{m}^2\cdot\text{K}$)
H_1	lower microchannel height (m)
H_2	upper microchannel height (m)
j	Colburn factor (-)
l	length (m)
L	length of the flow channel (m)
Nu	Nusselt number (-)
ΔP	pressure drop (Pa)
Pr	Prandtl number (-)
p	wetted perimeter (m)
q	heat flux (W/cm^2)
Re	Reynold number (-)
R	thermal resistance (K/W)
S	runner wetting area (m^2)
T	temperature (K)
ΔT	temperature difference (K)
u	inlet velocity (m/s)
V	liquid domain volume (m^3)
w	width (m)
Greek symbols	
ζ	comprehensive performance evaluation criteria (-)
λ	thermal conductivity ($\text{W}/\text{m}\cdot\text{K}$)
ρ	density (kg/m^3)
μ	dynamic viscosity ($\text{Pa}\cdot\text{s}$)
α	height ratio of the upper and lower microchannel (-)
Subscript	
av	average
b	base
c	channel
d	depth
eff	effective
in	inlet
i,j	tensor index symbols
max	maximum
min	minimum
out	outlet
r	rib
s	surface

References

1. Jahromi, P.F.; Karimi-Sabet, J.; Amini, Y.; Fadaei, H. Pressure-driven liquid-liquid separation in Y-shaped microfluidic junctions. *Chem. Eng. J.* **2017**, *328*, 1075–1086. [[CrossRef](#)]
2. Marsousi, S.; Karimi-Sabet, J.; Moosavian, M.A.; Amini, Y. Liquid-liquid extraction of calcium using ionic liquids in spiral microfluidics. *Chem. Eng. J.* **2018**, *356*, 492–505. [[CrossRef](#)]
3. Yang, Y.; Du, J.; Li, M.; Li, W.; Wang, Q.; Wen, B.; Zhang, C.; Jin, Y.; Wang, W. Embedded microfluidic cooling with compact double H type manifold microchannels for large-area high-power chips. *Int. J. Heat Mass Transf.* **2022**, *197*, 123340. [[CrossRef](#)]
4. Zhang, D.; Fu, L.; Guan, J.; Shen, C.; Tang, S. Investigation on the heat transfer and energy-saving performance of microchannel with cavities and extended surface. *Int. J. Heat Mass Transf.* **2022**, *189*, 122712. [[CrossRef](#)]
5. Moore, G.E. Cramming more components onto integrated circuits. Reprinted from *Electronics*, Volume 38, Number 8, April 19, 1965, p. 114. *IEEE Solid-State Circuits Newsl.* **2006**, *11*, 33–35. [[CrossRef](#)]
6. Mandel, R.K.; Bae, D.G.; Ohadi, M.M. Embedded Two-Phase Cooling of High Flux Electronics via Press-Fit and Bonded FEEDS Coolers. *J. Electron. Packag.* **2018**, *140*, 031003. [[CrossRef](#)]
7. Harpole, G.M.; Eninger, J.E. Micro-channel heat exchanger optimization. In Proceedings of the Seventh Annual IEEE Semiconductor Thermal Measurement and Management Symposium (SEMI-THERM VI), Phoenix, AZ, USA, 12–14 February 1991; pp. 59–63.
8. Li, Z.; Peng, Y.; Yang, X. The Experimental Study of the Performance of Zigzag Microchannel Exchanger. *Modul. Mach. Tool Autom. Manuf. Tech.* **2021**, *9*, 57–61.
9. Zhai, Y.; Xia, G.; Cui, Z. Numerical simulation of flow and heat transfer in spaced fan-shaped cavity microchannels. *J. Beijing Univ. Technol.* **2014**, *40*, 627–633.
10. Xu, S.; Guo, Z.; Qin, J.; Cai, Q.; Hu, G.; Wang, W. Bionic modeling of tree-shaped microchannel heat sink and numerical analysis of 3D heat flow characteristics. *China Mech. Eng.* **2014**, *25*, 1185–1188.
11. Li, Y.; Wu, H. Experiment investigation on flow boiling heat transfer in a bidirectional counter-flow microchannel heat sink. *Int. J. Heat Mass Transf.* **2022**, *187*, 122500. [[CrossRef](#)]
12. Alam, M.W.; Bhattacharyya, S.; Souayeh, B.; Dey, K.; Hammami, F.; Rahimi-Gorji, M.; Biswas, R. CPU heat sink cooling by triangular shape micro-pin-fin: Numerical study. *Int. Commun. Heat Mass Transf.* **2020**, *112*, 104455. [[CrossRef](#)]
13. Yang, D.; Yan, W.; Ding, G.; Jin, Z.; Zhao, J.; Wang, G. Numerical and experimental analysis of cooling performance of single-phase array microchannel heat sinks with different pin-fin configurations. *Appl. Therm. Eng.* **2017**, *112*, 1547–1556. [[CrossRef](#)]
14. Xia, G.; Cui, Z.; Zhai, Y.; Cui, Y.; Li, J. Flow and heat transfer characteristics of heat sink with rhomboid microneedle ribs. *J. China Univ. Pet.* **2014**, *38*, 130–134.
15. Ambreen, T.; Kim, M.H. Effect of fin shape on the thermal performance of nanofluid-cooled micro pin-fin heat sinks. *Int. J. Heat Mass Transf.* **2018**, *126*, 245–256. [[CrossRef](#)]
16. Vafai, K.; Zhu, L.U. Analysis of two-layered micro-channel heat sink concept in electronic cooling. *Int. J. Heat Mass Transf.* **1999**, *42*, 2287–2297. [[CrossRef](#)]
17. Hu, N.; Wang, Q.; Liu, S.; Gu, J.; Li, L.; Lyu, J. A narrow shape double-layer microchannel heat sink (DL-MCHS) designed for high-power laser crystal. *Appl. Therm. Eng. Des. Processes Equip. Econ.* **2022**, *211*, 118456. [[CrossRef](#)]
18. Lin, L.; Chen, Y.; Wang, X. Optimization of crucial parameters for double-layer microchannel heat sink. *J. Eng. Thermophys.* **2014**, *35*(3), 567–570.
19. Shen, H.; Xie, G.; Wang, C.C. Thermal performance and entropy generation of novel X-structured double layered microchannel heat sinks. *J. Taiwan Inst. Chem. Eng.* **2020**, *111*, 90–104. [[CrossRef](#)]
20. Chen, R.; Tang, S. Simulation of heat transfer performance of double-layer trapezoidal microchannel heat sink based on pyramidal perturbation structure. *Prog. Chem. Ind.* **2020**, *39*, 7.
21. Zhang, Y.D.; Chen, M.R.; Wu, J.H.; Hung, K.-S.; Wang, C.-C. Performance Improvement of a Double-Layer Microchannel Heat Sink via Novel Fin Geometry—A Numerical Study. *Energies* **2021**, *14*, 3585. [[CrossRef](#)]
22. Pan, Y.H.; Zhao, R.; Fan, X.H.; Nian, Y.-L.; Cheng, W.-L. Study on the effect of varying channel aspect ratio on heat transfer performance of manifold microchannel heat sink. *Int. J. Heat Mass Transf.* **2020**, *163*, 120461. [[CrossRef](#)]
23. Gan, T.; Quan, X. Numerical simulation of flow and heat transfer characteristics in a novel orifice plate manifold microchannel. *Cryogenics* **2019**, *5*, 59–63.
24. Yang, M.; Cao, B.Y. Multi-objective optimization of a hybrid microchannel heat sink combining manifold concept with secondary channels. *Appl. Therm. Eng.* **2020**, *181*, 115592. [[CrossRef](#)]
25. Gilmore, N.; Menictas, C.; Timchenko, V. Open manifold microchannel heat sink for high heat flux electronic cooling with a reduced pressure drop. *Int. J. Heat Mass Transf.* **2020**, *163*, 120395. [[CrossRef](#)]
26. Erp, R.V.; Soleimanzadeh, R.; Nela, L.; Kampitsis, G.; Matioli, E. Co-designing electronics with microfluidics for more sustainable cooling. *Nature* **2020**, *585*, 211–216. [[CrossRef](#)] [[PubMed](#)]
27. Song, J.Y.; Hah, S.; Kim, D.; Kim, S.-M. Enhanced flow uniformity in parallel mini-channels with pin-finned inlet header. *Appl. Therm. Eng.* **2019**, *152*, 718–733. [[CrossRef](#)]

28. Li, Y.; Qiu, Z.; Cui, D.; Wang, Z.; Zhang, J.; Ji, Y. Numerical investigation on the thermal-hydraulic performance of helical twine printed circuit heat exchanger. *Int. Commun. Heat Mass Transf.* **2021**, *128*, 105596. [[CrossRef](#)]
29. Drummond, K.P.; Back, D.; Sinanis, M.D.; Janes, D.B.; Peroulis, D.; Weibel, J.A.; Garimella, S.V. A hierarchical manifold microchannel heat sink array for high-heat-flux two-phase cooling of electronics. *Int. J. Heat Mass Transf.* **2018**, *117*, 319–330. [[CrossRef](#)]
30. Eslami, M.; Kamali, R.; Derakhshanpour, K. Improving performance of single and double-layered microchannel heat sinks by cylindrical ribs: A numerical investigation of geometric parameters. *Int. Commun. Heat Mass Transf. Rapid Commun. J.* **2021**, *126*, 105440.